Structural properties of narrow hexagonal MnAs nanowires: Role of edge atoms

Ali Kazempour, S. Javad Hashemifar, and Hadi Akbarzadeh
Department of Physics, Isfahan University of Technology, 84156-83111 Isfahan, Iran
(Received 15 December 2008; revised manuscript received 21 April 2009; published 18 May 2009)

First-principles pseudopotential calculations are employed to study the structural stability of hexagonal MnAs(0001) nanowires. The calculated total energies are combined with a phenomenological model to describe the energy of broken bonds at surfaces and edges. The obtained cohesive energies are fitted by appropriate equations of state to determine the edge and surface energies of various MnAs nanowires. We discuss that occurrence of Mn edges in these nanostructures is not favorable and rather these systems prefer to have sharp As edges. Our study on structural stability is extended to more realistic conditions by applying the *ab initio* atomistic thermodynamics procedure. The important influence of edges on the stability of the hexagonal MnAs nanowires is confirmed in all parts of our theoretical investigation.

DOI: 10.1103/PhysRevB.79.195420 PACS number(s): 73.22.−f, 61.46.−w

I. INTRODUCTION

Magnetic nanostructures are potential candidates for design and creation of novel nanotechnology devices and functionalities.[1,2] Finite size effects and quantum confinement have important influences on structural, electronic, magnetic, and optical properties of these systems.[3,4] Hence, quantum nanowires (NWs) are among attractive nanostructures for observing and studying innovative physical properties.

Ferromagnetic metallic MnAs nanostructures have recently attracted much attention due to their room-temperature magnetic properties, relatively small coercive field, and ease of growth on arsenide semiconductors.[1,2] Experimentalists grew MnAs thin films on GaAs(001) and observed in-plane regular arrays of ferromagnetic hexagonal α- and orthorhombic β-MnAs wires.[2,5–7] It has been shown that the width of the ferromagnetic wires can be continuously changed from isolated dot at high temperature to well-ordered NWs at lower temperature.[8] Moreover, Takagaki *et al.*[9] fabricated MnAs NWs at different crystallographic directions and found that the resistivity of narrow MnAs[0001] wires is smaller than MnAs $[11\bar{2}0]$ NWs.

Realization of the potential applications of NWs needs the accurate control of growth parameters and precise characterization methods being provided by modern expensive experimental setups such as scanning tunneling microscopy.[10] Density-functional theory (DFT) calculations are very helpful for finding an accurate microscopic understanding of the stable structural configuration and electronic structure. Hence our aim in this work is employing DFT computations for better understanding of MnAs nanowire's structural characteristic regardless of substrate. We combine first-principles total energies with appropriate phenomenological model to describe the stable structure of MnAs(0001) nanowires. In Sec. II the basic strategy and terminology of this paper are discussed in detail. Then we use the concept of dangling-bond (DB) energies to discuss the behavior of cohesive energies and extrapolate our results to larger scale NWs. In Sec. IV, the stability of MnAs(0001) NWs is discussed in terms of equation of states while in Sec. VIII an *ab initio* thermodynamic description based on chemical potentials is presented and appropriate phase diagrams are plotted.

II. COMPUTATIONAL DETAILS

A. Geometrical description of nanowires

Allen[11] argued that a nanocrystalline nanowire in the optimal configuration is a maximally linear cluster and grows around the symmetry axis of this cluster. Since the highest symmetry axes of the hexagonal MnAs in [0001] direction are vertical Mn and As arrays, therefore the most stable NWs are likely those with these vertical arrays as their central and growth axes. Therefore two general classes of MnAs(0001) nanowires were studied in the current work. In the first class a chain of Mn atoms makes the central axis of the nanowire and hence is called Mn center (MC) NWs while in the second class, which is named As center (AC) NWs, an As chain is the central axis of the nanowire.

Hexagonal MC NWs and AC NWs are the most symmetrical MnAs nanowires in (0001) direction. MC NWs have 24 symmetry operations while AC NWs due to the lack of inversion center have 12 symmetry operations. In Fig. 1 the three first diameters of the NWs within each class are sketched. As it is shown in the figure, the facets of these

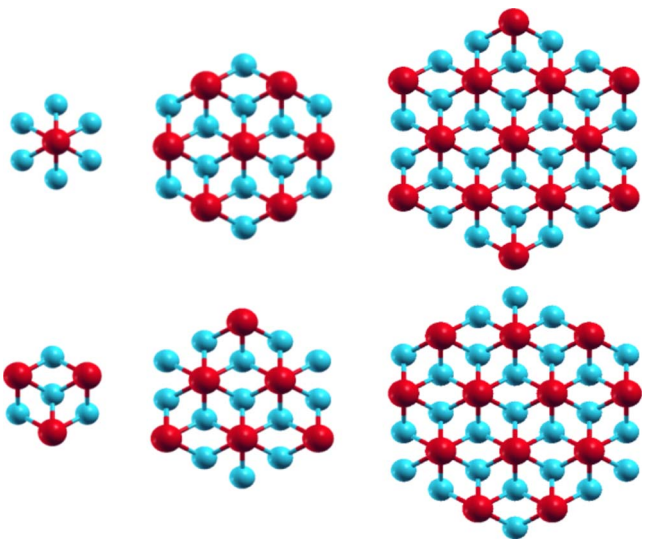

FIG. 1. (Color online) The first, second, and third diameter hexagonal MC and AC nanowires. The bigger symbols (red color) correspond to Mn atoms and the smaller ones (blue) indicate As atoms.

TABLE I. The geometrical parameters of the hexagonal MC and AC MnAs(0001) nanowires. Each class is divided into three types. k is an integer number including zero. As1 (As2) indicates As edges consisting of two (four) coordinated As atoms.

	MC			AC		
	Type 1	Type 2	Type 3	Type 1	Type 2	Type 3
Diameter	$3k+1$	$3k+2$	$3k+3$	$3k+1$	$3k+2$	$3k+3$
Edge composition	As1	As2	Mn	Mn+As2	Mn+As1	As1+As2
Number of Mn atoms at edges	0	0	12	6	6	0
Number of Mn atoms on facets	$12k$	$12(k+1)$	$12k$	$12k$	$12k$	$12(k+1)$
Number of As1 atoms at edges	6	0	0	0	3	3
Number of As2 atoms at edges	0	6	0	3	0	3
Number of As atoms on facets	$12k$	$12k$	$12(k+1)$	$12k$	$12k+6$	$12k+6$
Total number of surface atoms	$24k+6$	$24k+18$	$24(k+1)$	$24k+9$	$24k+15$	$24(k+1)$

NWs are portions of $(11\bar{2}0)$, $(10\bar{1}0)$, and $(01\bar{1}0)$ planes of hexagonal MnAs. Since these three planes are equivalent then the main parameter that makes NWs different is the places where the facets are cut or better saying the nanowire edges. In Sec. III, we will discuss that edge composition is the key controlling parameter of the stability of the hexagonal MnAs(0001) NWs. According to Fig. 1, in the first and second diameter MC NWs, edges are made of As atoms while in the third diameter MC NW, Mn chains make the edges. On the other hand, in the first and second diameter AC NWs, half of the edges are As chains and the other half are Mn chains while in the third diameter is AC NW, all edges are made of As chains. More precise consideration shows that two different kinds of As edges exist in the nanowires. The first kind (As1) consists of the four coordinated As atoms (e.g., edges of the first diameter MC NW) while in the second kind As edge (As2) arsenic atoms are two coordinated (e.g., the second diameter MC NW).

There is a periodicity of 3 in the edge composition of NWs versus diameter, meaning that the Rth and the $[R+3]$th diameter NWs have identical edge compositions. Therefore each class of NWs is divided into three types. The first type (type 1) in each class is the $[3k+1]$th diameters NWs (k is an integer number which starts from zero) which include, for example, the first ($k=0$) and fourth ($k=1$) diameter NWs. Similarly type 2 and type 3 are the $[3k+2]$th and $[3k+3]$th diameter NWs, respectively. Clearly, the first, second, and third diameter NWs shown in Fig. 1 are prototype examples of type 1, type 2, and type 3 NWs, respectively.

In order to address the structural stability of MnAs nanowires, we calculated four smallest diameters of MC NWs and AC NWs (Fig. 1). These simulations were done in the hexagonal supercells in which the nanowire is surrounded in the xy plane by a vacuum thickness of about 8.5 Å to prevent interaction between adjacent wires. We will use a phenomenological model to extrapolate results to larger scales and investigate stability of larger diameter NWs with almost no computational cost. In this model the cohesive energy of the system is expressed as a function of the number of surface atoms, hence a systematic method for counting the number of surface atoms as a function of NW diameter is very helpful.

After precise geometrical considerations, we formulated the number of different surface atoms as a function of diameter for all NW types. The results are summarized in Table I along with some other useful geometrical parameters of the nanowires. Moreover, the total number of atoms in the Rth diameter NW is formulated as the sum of number of surface atoms of all smaller NWs: $N_{\mathrm{tot}}(R)=N_s(R)+N_s(R-1)+\cdots+N_s(0)$, where $N_s(0)$ is 1 (2) for AC NWs (MC NWs).

B. Method of calculations

Our total energy calculation was performed by using QUANTUM ESPRESSO/PWSCF package[12] which is based on the density-functional theory and the ultrasoft pseudopotential techniques.[13] The Perdew, Burke, and Ernzerhof formalism of the generalized gradient approximation[14] to the exchange-correlation potential was used in this work. After doing enough convergence test, an energy cutoff of 30 Ry for plane-wave expansion and a mesh of $(1\times1\times8)$ **k** points for Brillouin zone integration were chosen for the nanowire calculations. All the structures have been optimized to achieve the minimum energy by accurate relaxation of the atomic positions down to the forces less than 1 mRy/bohr.

For better interpretation of the nanowire results, we studied the free MnAs $(10\bar{1}0)$ surfaces which are equivalent to all facets of the hexagonal MnAs nanowires. The corresponding supercell slab consists of seven atomic layers (equal to the number of atomic layers in the third diameter NWs) and a 20 bohrs thick vacuum region. The surface calculations were performed with the same accuracy as the nanowire calculations.

III. STRUCTURAL PROPERTIES

The atomic configurations of three narrowest MC NWs and AC NWs are presented in Fig. 1. Except for the third and fourth diameter NWs, the c lattice parameters of nanowires were optimized by calculating supercell energies at different values of c. By fitting a parabolic curve to the obtained total energy versus c data the structural properties of the NWs were calculated and listed in Table II. Comparing the optimized c lattice constant of the first and second diameter NWs

TABLE II. The structural properties of the four thinest MC and AC nanowires. MC-i (AC-i) indicates ith diameter MC NW (AC NW). $d^s_{\text{Mn-As}}$(Å): Mn-As bond length at the NW surface, $d^c_{\text{Mn-As}}$(Å): Mn-As bond length at the NW center, E_C (Ry): cohesive energy, Y (GPa): Young modulus, $\bar{m}_{\text{Mn}}(\mu_B)$: average magnetic moment of Mn atoms, and $\bar{m}_{\text{As}}(\mu_B)$: average magnetic moment of As atoms.

	DB ratio	Mn/As ratio	c	$d^s_{\text{Mn-As}}$	$d^c_{\text{Mn-As}}$	E_C	Y	$\bar{m}_{\text{Mn}}$	$\bar{m}_{\text{As}}$
Bulk		1	10.63	2.58	2.58	−0.256	46.9	3.59	−0.25
MC-1	4	0.33	8.93	2.38	2.38	−0.204	161.3	1.98	−0.15
MC-2	2	1.17	11.13	2.57	2.51	−0.224	58.9	3.85	−0.26
MC-3	2.5	1.08	10.63	2.44	2.58	−0.229		3.70	−0.26
MC-4	4	0.9	10.63	2.52, 2.36	2.56	−0.236		3.61	−0.26
AC-1	2.66	1.5	12.54	2.45, 2.50	2.45,2.50	−0.198	72.6	3.54	−0.32
AC-2	7.8	0.92	11.16	2.45, 2.53	2.57	−0.217	74.3	3.64	−0.28
AC-3	2.25	0.96	10.63	2.56, 2.54, 2.36	2.54	−0.232		3.63	−0.31
AC-4	3.81	1.05	10.63	2.51, 2.54	2.55	−0.236		3.62	−0.28

with bulk value, we clearly observe that by increasing the diameter this parameter approaches quickly to the bulk value. Hence we neglected c optimization for the third and forth diameter NWs and adopted the corresponding bulk values for these systems.

It is observed that all optimized c values of nanowires are larger than the bulk value except the first diameter MC NW. In order to discuss the behavior of this lattice constant, one should understand the kinds of surface effects that occur in the system. An important effect is the relaxation of the surface atoms which is due to the missed bonds at the surface. As it is visible in Table II, we find that in all studied NWs the Mn-As bond length at the surface is smaller than bulk. It evidences the inward relaxation and contraction of surface atoms in the xy plane that can induce an outward relaxation of the unit cell in the z direction. As it is visible in Fig. 2, this inward relaxation is more pronounced for the surface Mn than the surface As atoms. The second important surface effect is related to magnetism. Reduction in the coordination number of atoms at surfaces usually enhances exchange interaction and atomic magnetic moments. Since positive pressure, as a general trend, reduces atomic magnetic moments in crystals, hence magnetic enhancement may lead to a negative pressure and lattice expansion. We observed this behavior in all NWs except the first diameter MC NW that has a lower value of average magnetic moment compared to bulk. Since this nanowire has no surface Mn atom, it has the highest unstoichiometry and lowest Mn/As ratio compared to bulk and other nanowires (Table II). Therefore its magnetization is substantially lower than the bulk value, compensating the effect of inward planner relaxation and leading to reduction in c lattice parameter compared to bulk. The presence of surface Mn in other nanowires leads to an enhanced magnetization which along with inward relaxation of atoms in the xy plane is the main origin of the expansion of c lattice constant in the nanostructures.

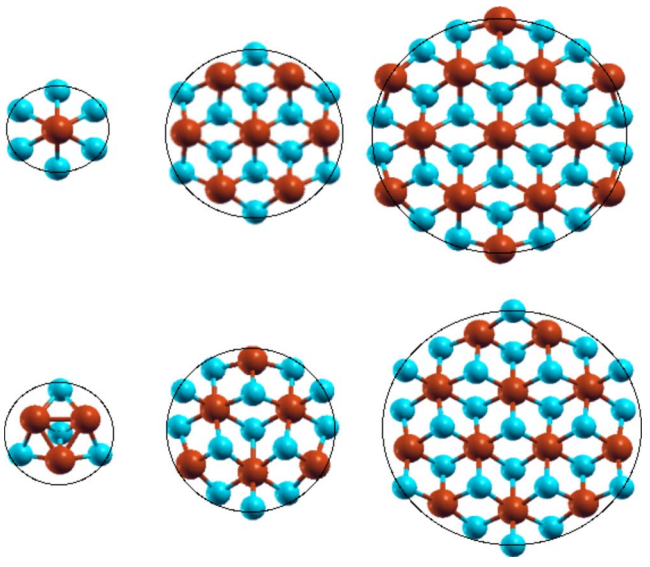

FIG. 2. (Color online) The relaxed structure of the first, second, and third diameter MC (top) and AC (bottom) nanowires.

The stability of NWs is discussed in terms of the cohesive energy E_C defined as

$$E_C = (E_{\text{tot}} - N_{\text{Mn}}\mu_{\text{Mn}} - N_{\text{As}}\mu_{\text{As}})/N_{\text{tot}}, \quad (1)$$

where E_{tot} is the NW total energy and N and μ are the number of atoms and isolated atomic energies. The calculated E_C for the studied NWs is listed in Table II. It is observed that in the first and second diameter NWs, MC wires are more stable while in the third diameter, AC NW is more favored. The common feature of the stable nanowires is that all of them have no Mn chain at their edges. It seems that presence of Mn atoms at the edges is not favored in the MnAs nanowires. The Mn atoms at the lateral facets have two broken bonds while at the edges they have three broken bonds compared to the bulk and hence are more unstable. As it is expected, we find that by increasing the NW diameter, due to the reduction in the relative contribution of the surface dangling bonds, E_C converges to the corresponding bulk value.

IV. MICROSCOPIC DESCRIPTION OF COHESIVE ENERGY

At the following, a phenomenological model is introduced which expresses the cohesive energy of nanowires as a function of dangling-bond energies. The DB energies are phe-

TABLE III. The obtained dangling bond energies (mRyd). The superscripts **0** indicate the first diameter nanowires.

$\varepsilon_b^{2a_0}$	$\varepsilon_b^{3m_0}$	ε_b^{2a}	ε_b^{3m}	ε_b^{4a}	ε_b^{4m}
−17.33	−26.85	−23.22	−25.12	−14.86	−25.39

nomenological parameters which measure the energy of the broken bonds at surfaces and are determined by fitting the following model to the calculated cohesive energies of some narrower NWs. This model enables us to extrapolate the results to large scales and calculate the cohesive energy of large diameter NWs without any further time consuming first-principles calculations on these systems.

In order to apply this model to our case, first the various dangling bonds at the surfaces of MnAs[0001] nanowires should be distinguished. In the bulk hexagonal MnAs, both Mn and As atoms are six coordinated while at the nanowire lateral facets and edges, Mn and As atoms are three or four and two or four coordinated, respectively. Hence the model cohesive energy (E_C^{mod}) could be formulated as follows:[15]

$$E_C^{\text{mod}} = E_0 - \frac{1}{N_{\text{tot}}}(N^{4m}\varepsilon_b^{4m} + N^{4a}\varepsilon_b^{4a} + N^{2a}\varepsilon_b^{2a} + N^{3m}\varepsilon_b^{3m}), \tag{2}$$

where E_0 is the bulk cohesive energy, $N^{\beta x}$ is the number of dangling bonds of all β-coordinated x atoms (m and a in place of x stand for Mn and As atoms), and $\varepsilon_b^{\beta x}$ is energy of a broken (dangling) bond of β-coordinated x atom. By fitting the above model to the cohesive energies of eight calculated NWs, the phenomenological dangling-bond energies will be determined and then used to calculate the cohesive energy of larger NWs. For better fitting to the calculated data, ε_b^{2a} and ε_b^{3m} of the first diameter nanowire are allowed to be independent of other diameters. The obtained DB energies after the best fit are listed in Table III. It should be mentioned that the transferability of the obtained dangling-bond energies is not guaranteed for very large diameter NWs.

It is observed that $\varepsilon_b^{3m_0}$ and ε_b^{3m} are close together while $\varepsilon_b^{2a_0}$ is much lower than ε_b^{2a}. It is in well agreement with the structural properties presented in Table II. $\varepsilon_b^{3m_0}$ is the DB energy of Mn at the surface of first diameter AC NW while $\varepsilon_b^{2a_0}$ is the DB energy of As at the surface of first diameter MC NW. It was discussed that the first diameter MC NW, due to very low Mn/As ratio, is quite different to the other nanowires (much lower c lattice parameter and magnetic moment and much higher Young's modulus). Hence the DB energy of two coordinated As atoms at its surface ($\varepsilon_b^{2a_0}$) is substantially lower than the other NWs (ε_b^{2a}). In contrast, the first diameter AC NW has rather similar properties to the other NWs and hence the three coordinated surface Mn atoms have similar DB energies on all NWs. Moreover, it was found that the DB energies of four coordinated Mn and As atoms are not equal (Table III), indicating more energy cost of bond breaking for Mn atoms compared to As. It may explain more inward relaxation of the surface Mn atoms in the xy plane (see bond lengths in Table II).

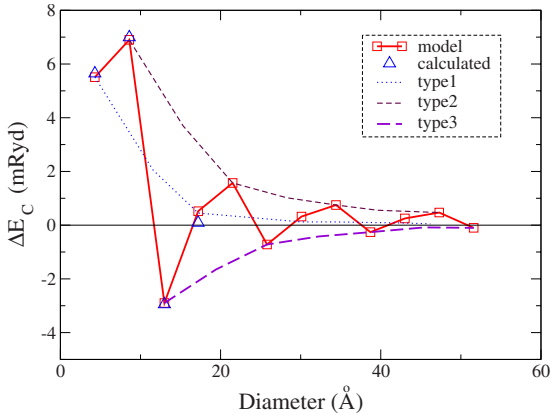

FIG. 3. (Color online) The cohesive-energy difference of AC and MC nanowires as a function of diameter. The upper and lower panels show the stable MC NWs and AC NWs, respectively.

We used the obtained dangling-bond energies and Eq. (2) to calculate the cohesive energies of large diameter MC and AC nanowires. The $N^{\beta x}$ parameters for large diameter NWs are calculated by using the given formulas in Table I and taking into account that the coordination number of Mn atom at facet (edge) is four (three), As at facet and As1 at edge are four, and As2 at edge is two. The extrapolated results were used to calculate the difference between cohesive energy of MC and AC NWs (ΔE_C) as a function of diameter (shown in Fig. 3). If ΔE_C is positive (the top part of the graph) then MC NW is more stable while in the bottom part of the graph, AC NW is more stable.

As it is expected, with increasing diameter the contribution of surface and DB energies decreases and cohesive energy approaches to the bulk value and then the cohesive-energy difference goes to zero. For the first three diameter NWs, the extrapolated cohesive energies coincide well with the calculated data, confirming the high accuracy of fitting. An interesting result which is obvious in the figure is that in the MC class, type 1 and type 2 NWs are more stable while in the AC class, type 3 NWs are energetically more favorable. Similar to Sec. III, the common geometrical property of all stable NWs the is absence of Mn atoms at their edges. We conclude that occurrence of Mn edges in the hexagonal MnAs(0001) nanowires is very unlikely specially in very small diameters. It is the reason behind the visible *two by one* periodicity of the cohesive-energy differences in Fig. 3. Clearly and reasonably, at very large diameters, the cohesive-energy difference between NWs vanishes and hence from theoretical point of view different types and classes of nanowires may coexist.

V. EQUATION OF STATE

In Sec. IV, atom-dependent phenomenological parameters (dangling-bond energies) were used to describe the behavior of cohesive energies, while here we analyze the stability of the hexagonal MnAs(0001) nanowires in terms of the system-dependent phenomenological parameters; surface and edge energies. Quantitatively, we split the NW cohesive

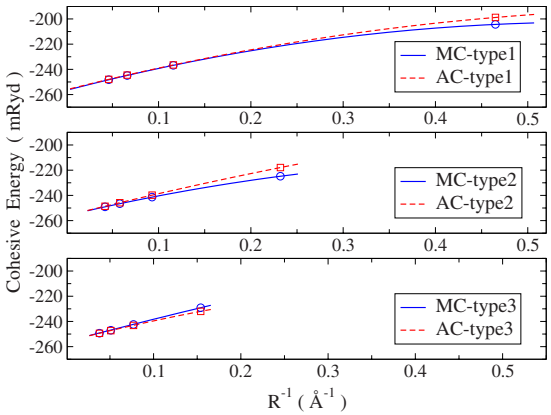

FIG. 4. (Color online) The extrapolated cohesive energy for all three types of MC NWs and AC NWs as a function of inverse radius.

energy per atom into three contributions: the bulk, surface, and edge energies

$$E_c = E_{\text{bulk}} + E_{\text{surface}} + E_{\text{edge}}, \tag{3}$$

where E_{edge} is the required energy for creation of an edge or equivalently matching two facets. It can affect surface reconstruction and electronic structure of NWs (Ref. 16) and even favor change in the E_{bulk}.[17] In the large scales, clearly, surface energy dominates the minor-edge contributions to the cohesive energy while for sufficiently small nanowires edges become important and hence a key issue is identification of the scale at which this happens.[16]

The above model equation has been used to explain structural stability and phase transitions in metallic and silicon nanowires.[17,18] We use this model to determine the surface and edge energies of various types of MnAs nanowires.

We define the parameters $\bar{\gamma}$, surface energy per atom per surface unit area averaged on all facets, and $\bar{\mu}$, edge energy per atom per unit length averaged on all edges, to rewrite Eq. (3) as follows:[18,19]

$$E_c(R) = E_{\text{Bulk}} + \frac{2R_0\Omega_c}{R}\bar{\gamma} + \frac{\Omega_c N}{\pi R^2}\bar{\mu}, \tag{4}$$

where $R_0 = 1.05$ is the actual perimeter of the hexagonal cross section divided by perimeter of a circle with the same area, N is number of edges (=6 for hexagonal NW), and Ω_c is the volume per atom of the bulk crystal. We used Eq. (2) and the obtained dangling-bond energies in Sec. IV to extrapolate the cohesive energy of the studied NWs at several diameters. The obtained cohesive energy data were fitted by Eq. (4) to determine the surface and edge energy mean values. The extrapolated data and fitted plots are presented in Fig. 4 and the determined $\bar{\gamma}$ and $\bar{\mu}$ values are listed in Table IV. It is evident in the figure that the cohesive energy scales linearly with R^{-1} at large diameters which indicates dominance of the surface contribution. While at small diameters, due to the importance of edge energies, the behavior deviates from linear scaling.

The obtained $\bar{\gamma}$ values are in agreement with the calculated surface energy of the free MnAs $(10\bar{1}0)$ surface

TABLE IV. The calculated mean values of the surface energy $\bar{\gamma}$(mRy/Å^2) and edge energy $\bar{\mu}$(mRy/Å) of the MnAs(0001) nanowires. The last row (edge) shows edge compositions which are taken from Table I. In this row *A* and *M* stand for As and Mn atoms.

	MC NW			AC NW		
	Type 1	Type 2	Type 3	Type 1	Type 2	Type 3
$\bar{\gamma}$	5.2	4.9	5.1	5.1	5.1	5.2
$\bar{\mu}$	−5.0	−5.5	−1.6	−3.9	−2.4	−5.5
Edge	*A*1	*A*2	*M*	*M*+*A*2	*M*+*A*1	*A*1+*A*2

(5.37 mRy/Å^2) which confirm the validity of the employed equation-of-state model. The small differences between $\bar{\gamma}$ values and free surface energy are due to the edge and finite size effects in the NWs.

According to Table IV, all $\bar{\mu}$ values are found to be negative which is inconsistent with the edge-energy concept. As it is noticed by Pelaez and Serena,[19] the origin of this inconsistency is in the fact that in Eq. (4) the corner atoms are contributing in both surface and edge energy terms. In order to correct this unphysical behavior, we used a new equation of state proposed by Pelaez and Serena[19]

$$E_c(R) = E_{\text{Bulk}} + \frac{N_{\text{sur}}A}{N_{\text{tot}}}\bar{\gamma} + \frac{N_{\text{edge}}L}{N_{\text{tot}}}\bar{\mu}, \tag{5}$$

where N_{sur} and N_{edge} are the total numbers of surface and edge atoms in the NW, A is the surface area per atom, and L is the length per edge atom in the NW. In this model the surface and edge atoms are directly counted and hence surface energy is better described. The E_{Bulk} and $\bar{\gamma}$ values are taken from separate bulk and free surface calculations and then entered into Eq. (5) to determine the edge energy as a function of NW diameter. The obtained results are plotted in Fig. 5. We observe that the new model properly determines positive edge energies. According to the results, the edge energies become very small for NW diameters bigger than 12 Å. It may be due to the possible inaccuracies, mentioned in Sec. IV, in the extrapolated cohesive energies of larger NWs.

The behavior of edge energies is very similar to the behavior of NW cohesive energies presented in Fig. 3. The

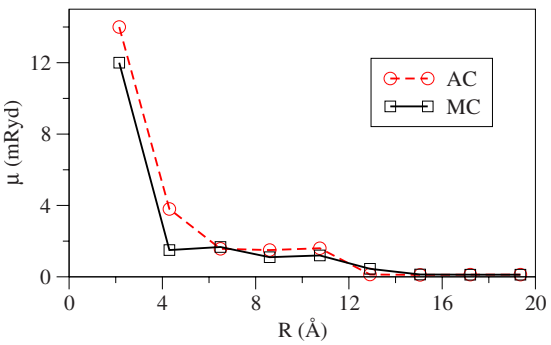

FIG. 5. (Color online) The calculated mean-edge energies as a function of NW diameter for MC and AC nanowires.

NWs with lower cohesive energy in Fig. 3 have lower edge energy in Fig. 5. Inspecting the atomic composition of the edges at each diameter, in Fig. 5, indicates that Mn edges have always higher energy than As edges. Hence, it is again argued that the formation of Mn edges in the hexagonal MnAs nanowires is not likely. The reason is that Mn is a cation in MnAs. For undercoordinated cation, it seems to have empty dangling bonds and adopt a planar configuration. It explains why Mn does not like edge site. For undercoordinated anion (As), it seems to have a fully occupied lone pair in a nonplanar configuration such as edge configuration.

As it is visible in Fig. 2, relaxation process smoothens edges of the first and second diameter AC NWs and third diameter MC NW while the edges of the first and second diameter MC NWs and third diameter AC NW are sharpened after relaxation. These interesting phenomena are explained well by the above statements about situation of undercoordinated cation and anion atoms at surface. The NW structures prefer to smoothen the cation Mn edges and sharpen the anion As edges.

As the final message of this section, we quote the title of a recent Nature Materials publication entitled *Edge atoms do all the work*.[20] In this paper, Kuch[20] argued that the edge atoms control magnetic anisotropy properties of Co nanostructures. In this section, it was justified that the structural stability of narrow hexagonal MnAs(0001) nanowires is mainly controlled by the edge atoms.

VI. PHASE DIAGRAM

In this section we use *ab initio* atomistic thermodynamics to address the stability of MnAs nanowires in a more realistic condition (elevated temperature and pressure).[21] Although in the nanowire growth, kinetics rather than thermodynamics dominates. However, prior to any kinetic study one has to consider what is thermodynamically feasible. In the *ab initio* atomistic thermodynamics approach, the grand-canonicals-based free energy (Γ) is identified as the proper thermodynamical-potential governing stability of systems

$$\Gamma = G(T,P) - \sum_i n_i \mu_i(T,P), \tag{6}$$

where G is the Gibbs free energy per atom and n_i and μ_i are the fractional number and chemical potential of the ith element which i runs over Mn and As atoms. Since the chemical potentials are experimentally controllable, hence the obtained phase diagrams in this method are helpful to find out the required growth conditions for stabilizing a nanowire with the desired surface structure.[22–24] In practice nanowires are thick enough to have bulklike central layers acting as a thermodynamic reservoir. Hence nanowire surfaces are in thermodynamic equilibrium with central bulk layers, $\mu_{\mathrm{Mn}} + \mu_{\mathrm{As}} = g_b$, where g_b is the Gibbs free energy of bulk MnAs. In order to fulfill this equilibrium conditions, the first and second diameter NWs are excluded from our thermodynamic studies. Inspecting the atomic partial density of states of the third diameter NWs indicates that the NW central layers have similar properties to the bulk MnAs.

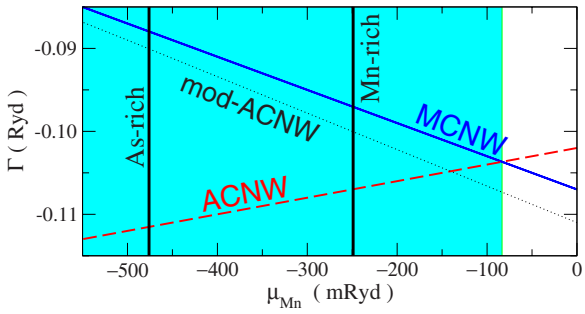

FIG. 6. (Color online) Phase diagram of the third diameter MC NW (solid line) and AC NW (dashed line). The different shaded areas show range of stability of each NW and vertical thick lines are corresponding boundaries to rich and poor Mn limits. Dotted line shows the Γ free energy of the modified structure of the third diameter AC NW (see Sec. VII).

It is argued that at sufficiently small temperatures, where vibrational contributions to the Gibbs free energy are neglectable; the static DFT total energies may be used as the input data for Eq. (6).[25] Imposing the above-mentioned thermodynamic equilibrium leaves only one independent chemical potential in Γ which is selected to be μ_{Mn}. The value of μ_{Mn} is practically bounded to the As-rich and Mn-rich boundaries which correspond to the formation of bulk Mn and As structures.[26] Following the above-mentioned scheme, we calculated Γ free energy of the third diameter MC NW and AC NW and plotted the resulted phase diagram in Fig. 6.

Obviously, the third diameter MC NW is stable in high μ_{Mn} while the third diameter AC NW is stable in lower μ_{Mn} values. It is attributed to the higher Mn/As ratio in the third diameter MC NWs (Table II). It is observed that the whole accessible region of the phase diagram which is limited by the rich and poor Mn boundaries is occupied by the third diameter AC NW. It indicates that the third diameter MC NW is not practically feasible.

In order to investigate the effects of NW size and type on the phase diagram, we used the extrapolated cohesive energies of the large NWs to calculate phase diagram of all types of MC and AC NWs at three different diameters. The obtained phase diagrams are plotted in Fig. 7. Accurate inspection of the plots shows that for each type of MnAs NWs, by increasing diameter the slope and the values at $\mu_{\mathrm{Mn}}=0$ of the Γ free energies decrease. According to Eq. (6) and the imposed thermodynamic equilibrium between surface and central part of NW, the slope of Γ is equal to the fractional number of surface Mn atoms which clearly decreases by increasing NW diameter. While the values of Γ at $\mu_{\mathrm{Mn}}=0$ are related to the cohesive energies of NWs which scale with $1/R$ at large diameters [Eq. (4)]. But the general phase diagram properties, namely, crossing points of MC and AC NW free energies and the stable phase in the accessible regions, are obviously similar for the same types of NWs. The stable phases of type 1 and type 2 NWs are always MC NW while AC NWs occupy whole accessible region of the type 3 NWs phase diagram, in well agreement with the results of Sec. V. Size-independent and type-dependent phase diagram properties are periodic features of the hexagonal MnAs nanowire which originated from geometrical periodicity of these systems described in Sec. II.

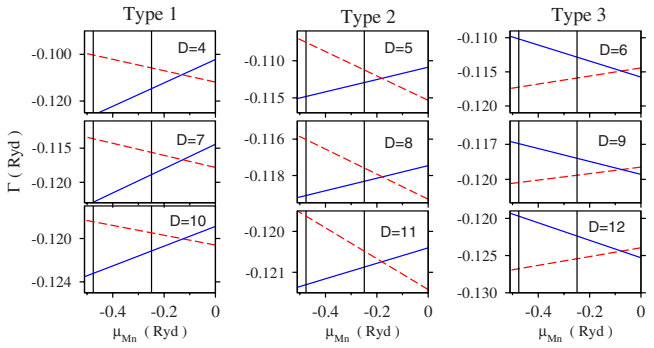

FIG. 7. (Color online) Phase diagrams of large diameters MnAs(0001) MC (solid line) and AC NWs (dashed line). The parameter D in each plot denotes the diameter of the corresponding nanowires. Vertical lines in all graphs show As and Mn rich boundaries (the same as Fig. 6).

VII. POSSIBLE STRUCTURAL DEFORMATIONS

The most part of our first-principles investigation was devoted to the ideal hexagonal shape MnAs(0001) NWs. In this short section we consider two possible structural modifications. According to Sec. VI, formations of Mn edges in the MnAs NWs are not desirable and stable NWs have only As edges. Two kinds of As edges may happen in this nanostructures; As1 and As2 edges. As2 atoms are four bonded As with the lowest dangling-bond energy (Table III) and hence form the most stable edge in the MnAs NWs (Table IV). In contrast, As1 atoms have the highest number of broken bonds among surface atoms. They have two bonds and four broken bonds. Hence removing these edge atoms will reduce the total number of dangling bonds and therefore may enhance cohesive energy and stability of the system.

In order to verify this prediction, we removed the As1 edges of the stable third diameter AC NW and calculated the total energy of the modified NW after full relaxation of the atomic positions. It was found that the cohesive energy of the modified NW (−0.233 Ry) is slightly less than the ideal NW (−0.232 Ry, Table II), indicating more or less stability of the modified wire. But after considering and plotting the Γ free energy of the modified NW (Fig. 6), we realized that this structure is unstable in the whole accessible region of the phase diagram. Therefore we conclude that although As1 atoms have four dangling bonds, removing these atoms will increase considerably the Mn/As ratio and hence seem undesirable.

Another possible structural deformation that may alter the core picture of this study is surface reconstruction. Although investigation of this phenomenon is out of the scope of the current study, the following qualitative arguments enhance the reliability of our results. It is argued that surface reconstruction is an important mechanism of energy lowering at semiconductor surfaces with covalent bonding while in metals and ionic crystals lowering of the surface energy is mainly achieved through relaxation of the surface atoms.[27] Therefore, in the hexagonal MnAs NWs which have metallic character, surface reconstruction has likely no profound influence on the relative cohesive energies of NWs. In addition, as it was mentioned in Sec. II, the facets of all studied nanowires are portions of $(11\bar{2}0)$, $(10\bar{1}0)$, and $(01\bar{1}0)$ planes of hexagonal MnAs. Since these planes are crystallographically equivalent, surface reconstruction may not significantly alter the presented energetic pictures in Sec. VI.

VIII. SUMMARY

In this paper we studied pristine hexagonal Mn center and As center MnAs(0001) nanowires by using density-functional pseudopotential calculations. The phenomenological parameter dangling-bond energies were used for microscopic description of nanowire cohesive energies. The obtained cohesive energies were entered into two equation-of-state models to determine the edge contributions to the cohesive energy of the nanowires. The obtained results enable us for a qualitative estimation of the energetically favorable edges. We concluded that hexagonal MnAs(0001) nanowires prefer sharp As edges whereas occurrence of Mn edges in these systems is unlikely. This behavior was attributed to the cationic character of Mn atoms which prefer planner configuration at surface while undercoordinated anion As atoms would like to have fully occupied lone pairs in a nonplanar configuration. By applying the *ab initio* atomistic thermodynamics and plotting appropriate phase diagrams, the structural stability of MnAs nanowires was discussed in a more realistic condition. The possibility of a structural deformation from hexagonal geometry was considered and found to be unfavorable.

ACKNOWLEDGMENTS

This work was supported jointly by the Vice Chancellor for Research Affairs of Isfahan University of Technology, Center of Excellence for Environmental nanotechnology, and ICTP Affiliated Centre. We thank our colleague Mojtaba Alaei for helpful discussions. S.J.H. gratefully appreciates financial support from the Alexander von Humboldt Stiftung and Peter Kratzer during his visits to Universität Duisburg-Essen, Duisburg, Germany.

[1] S. Datta and B. Das, Appl. Phys. Lett. **56**, 665 (1990).
[2] L. Daweritz, Rep. Prog. Phys. **69**, 2581 (2006).
[3] A. Nakamura, M. Brandbyge, L. B. Hansen, and K. W. Jacobsen, Phys. Rev. Lett. **82**, 1538 (1999).
[4] N. Akman, E. Durgun, S. Cahangirov, and S. Ciraci, Phys. Rev. B **76**, 245427 (2007).
[5] T. Plake, M. Ramsteiner, V. M. Kaganer, B. Jenichen, M. Kastner, L. Daweritz, and K. H. Ploog, Appl. Phys. Lett. **80**, 2523 (2002).
[6] B. Jenichen, V. M. Kaganer, M. Kastner, C. Herrmann, L. Daw-

eritz, K. H. Ploog, N. Darowski, and I. Zizak, Phys. Rev. B **68**, 132301 (2003).
[7] K. H. Ploog, J. Cryst. Growth **268**, 329 (2004).
[8] T. Plake, T. Hesjedal, J. Mohanty, L. Daweritz, and K. H. Ploog, Appl. Phys. Lett. **82**, 2308 (2003).
[9] Y. Takagaki, E. Wiebicke, L. Daweritz, and K. H. Ploog, J. Solid State Chem. **179**, 2271 (2006).
[10] A. L.-Y. N. Agrait and J. Ruitenbeek, Phys. Rep. **377**, 81 (2003).
[11] P. B. Allen, Nano Lett. **7**, 6 (2007).
[12] QUANTUM-ESPRESSO is a community project for high-quality QUANTUM-SIMULATION software, based on density-functional theory, and coordinated by Paolo Giannozzi. See http://www.quantum-espresso.org and http://www.pwscf.org
[13] For As pseudopotential, we used AS.PBE-VAN.UPF from the http://www.quantum-espresso.org distribution while for Mn, we generated an ultrasoft pseudopotential by using LD1 program of QUANTUM-ESPRESSO distribution and checked it by comparing some bulk data to full potential WIEN2K results.
[14] J. P. Perdew, K. Burke, and M. Ernzerhof, Phys. Rev. Lett. **77**, 3865 (1996).
[15] T. Akiyama, K. Nakamura, and T. Ito, Phys. Rev. B **73**, 235308 (2006).
[16] S. Ismail-Beigi and T. Arias, Phys. Rev. B **57**, 11923 (1998).
[17] Y. Zhao and B. I. Yakobson, Phys. Rev. Lett. **91**, 035501 (2003).
[18] O. Gulseren, F. Ercolessi, and E. Tosatti, Phys. Rev. Lett. **80**, 3775 (1998).
[19] S. Pelaez and P. A. Serena, Surf. Sci. **601**, 4163 (2007).
[20] W. Kuch, Nature Mater. **2**, 505 (2003).
[21] K. Reuter, C. Stampfl, and M. Scheffler, in *Handbook of Materials Modeling*, edited by S. Yip (Kluwer, Dordrecht, 2004), and references therein; http://www.fhi-berlin.mpg.de/th/pub04.html
[22] R. H. Miwa, T. M. Schmidt, and A. Fazzio, Phys. Rev. B **75**, 165324 (2007).
[23] R. Leitsmann and F. Bechstedt, J. Appl. Phys. **102**, 063528 (2007).
[24] E. Tosatti, Solid State Commun. **135**, 610 (2005).
[25] K. Reuter and M. Scheffler, Phys. Rev. B **65**, 035406 (2001).
[26] For a detailed description of phase diagram boundaries see Ref. 25. In order to determine the boundaries we calculated the minimized ground state energy of bulk As and for the complicated magnetic ground state of bulk Mn (α-Mn). We applied a correction taken from Ref. 28 to our calculated energy of antiferromagnetic γ-Mn to obtain the true ground state energy of α-Mn.
[27] *Encyclopedic Dictionary of Condensed Matter Physics*, edited by C. P. Poole, Jr. (Elsevier, San Diego, CA, 2004), Vol. 1.
[28] J. Hafner and D. Hobbs, Phys. Rev. B **68**, 014408 (2003).